






RESEARCH ARTICLE

Isotope effect suggests site-specific nonadiabaticity on Ge(111)c(2×8)

Kerstin Krüger¹  | Yingqi Wang^{2,3} | Lingjun Zhu⁴ | Bin Jiang⁴  | Hua Guo^{2,3}  | Alec M. Wodtke^{1,5,6}  | Oliver Bünermann^{1,5,6} 

¹Institute of Physical Chemistry, Georg-August University, Göttingen, Germany

²Department of Chemistry and Chemical Biology, University of New Mexico, Albuquerque, New Mexico, USA

³Center for Computational Chemistry, University of New Mexico, Albuquerque, New Mexico, USA

⁴Key Laboratory of Precision and Intelligent Chemistry, Department of Chemical Physics, University of Science and Technology of China, Hefei, China

⁵Department of Dynamics at Surfaces, Max-Planck-Institute for Multidisciplinary Sciences, Göttingen, Germany

⁶International Center of Advanced Studies of Energy Conversion, Georg-August University, Göttingen, Germany

Correspondence

Oliver Bünermann, Institute of Physical Chemistry, Georg-August University, Göttingen, Germany.

Email:

oliver.buenermann@chemie.uni-goettingen.de

Funding information

Max-Planck-Gesellschaft; Deutsche Forschungsgemeinschaft, Grant/Award Numbers: INST 186/902-1, SFB1073, projectA04(217133147); National Science Foundation, Grant/Award Numbers: CHE-1951328, CHE-2306975; Volkswagen Foundation, Grant/Award Number: INST 186/902-1; Niedersächsisches Ministerium für Wissenschaft und Kultur, Grant/Award Number: INST 186/902-1; Alexander von Humboldt-Stiftung; K. C. Wong Education Foundation, Grant/Award Number: GJTD-2020-15

Abstract

Energy transferred in atom-surface collisions typically depends strongly on projectile mass, an effect that can be experimentally detected by isotopic substitution. In this work, we present measurements of inelastic H and D atom scattering from a semiconducting Ge(111)c(2×8) surface exhibiting two scattering channels. The first channel shows the expected isotope effect and is quantitatively reproduced by electronically adiabatic molecular dynamics simulations. The second channel involves electronic excitations of the solid and, surprisingly, exhibits almost no isotope effect. We attribute these observations to scattering dynamics, wherein the likelihood of electronic excitation varies with the impact site engaged in the interaction.

Key Points

- Previous work revealed that H atoms with sufficient translational energy can excite electrons over the band gap of a semiconductor in a surface collision.
- We studied the isotope effect of the energy transfer by H/D substitution and performed band structure calculations to elucidate the underlying excitation mechanism.
- Our results suggest a site-specific mechanism that requires the atom to hit a specific surface site to excite an electron-hole pair.

KEYWORDS

Born–Oppenheimer failure, H atom, isotope effect, semiconductor, surface dynamics

This is an open access article under the terms of the [Creative Commons Attribution](https://creativecommons.org/licenses/by/4.0/) License, which permits use, distribution and reproduction in any medium, provided the original work is properly cited.

© 2023 The Authors. *Natural Sciences* published by Wiley-VCH GmbH.

INTRODUCTION

A common experimental approach to elucidate reaction, scattering, and energy transfer mechanisms of atom–surface interactions employs the isotope effect, usually using H/D substitution.^{1–9} Dependent on the underlying mechanism, different responses of the system to isotopic substitution are found. Inelastic scattering may result from mechanical excitation of lattice vibrations (phonons) by the impinging projectile. Here, the influence of isotopic substitution on energy transfer can be understood as the result of momentum conservation and D will transfer more energy than H. This behavior is seen for scattering from an insulator surface, where the energy loss of D atoms is about two times larger than for H atoms.¹⁰ Alternatively, electron-hole-pairs (EHPs) can be excited by the collision via an electronic friction mechanism¹¹; here, iso-energetic H and D impinge at the surface with different velocities, resulting in reduced friction and reduced energy transfer for D compared to H. For example, strong isotope effects are observed in chemicurrent measurements,^{5,12–15} where ultrathin metal film Schottky diode detectors enable the direct detection of electronic excitation that results from chemisorption. Here, deuterium-induced chemicurrents are two to five times smaller than those measured with H atom exposure. In fact, both isotope effects are present in inelastic scattering experiments from metals,^{8,16,17} where a reduced isotope effect is due to compensation of two mass-dependent effects on the energy transfer: an increased energy loss to the phonon system and a decreased energy loss to electronic excitation for D compared to H.

In a recent study on H atom scattering from the semiconducting, reconstructed Ge(111)c(2×8) surface, a bimodal energy-loss distribution was observed when the incident translational energy exceeds the energy of the surface band gap.¹⁸ One channel, which is present for translational energies both above and below the band gap, could be well described by an electronically adiabatic molecular dynamics (MD) simulation, whereas, until now, there are no theoretical models, including an electronic friction model capable of describing the second channel, which only emerges when translational energies exceed the surface band gap.¹⁹ Due to its large energy loss with an onset close to the surface band gap and its absence in the adiabatic simulations, the second channel was assigned to an electronically nonadiabatic process leading to the excitation of a surface electron across the surface band gap.

The goal of the present work is to provide further insights into the scattering dynamics by studying the isotope effect. This approach helps to confirm the previous conclusions of the adiabatic behavior of the first scattering channel; it also serves to help us gain a deeper understanding of the nature of the second nonadiabatic channel. In particular, we present translational energy-loss measurements of D atoms scattered from Ge(111)c(2×8) with incidence translational energies of about 1 and 2 eV and compare them to H atom scattering with similar incidence energies. The experiments reveal bimodal energy-loss distributions for D that are very similar to those for H; one scattering channel exhibits low energy loss, while the other one transfers much more energy to the surface. The experimental results are further compared to electronically adiabatic MD simulations, which were

performed using a high-dimensional neural network potential energy surface (NN-PES). MD simulations reproduce the energy-loss distribution for both isotopes, but only for one of the two scattering channels. Comparing the results of H to D atom scattering reveals that the adiabatic channel shows an isotope effect matching the prediction for an adiabatic energy transfer mechanism. In contrast, nearly no isotope effect is observed for the second, nonadiabatic channel. The results give further insights into the properties of the second channel suggesting the importance of site-specific nonadiabatic coupling.

METHODS

Experimental methods

The experimental setup is described in detail in Refs. 20, 21. In short, an H or D atomic beam with translational energies of $E_{i,H} = 0.99$ and 1.92 eV or $E_{i,D} = 0.94$ and 1.87 eV, is produced by ultraviolet photodissociation ($\lambda_{\text{photolysis}} = 248.35$ nm) of a supersonic molecular beam of hydrogen iodide or deuterium iodide, respectively. The H or D atom beam passes two differential pumping chambers to enter an ultra-high vacuum scattering chamber before colliding with the germanium crystal. The Ge sample is mounted on a 5-axis manipulator allowing the variation of the polar incidence angle ϑ_i with respect to the surface normal. The translational energy and angular distributions of the scattered H or D atoms are detected by Rydberg atom tagging time-of-flight. Here, the atoms are excited to a long-lived Rydberg state just below the ionization limit,²² pass a distance of 250 mm, are field-ionized, and then detected by a multichannel plate assembly. A multichannel scaler records the arrival time to obtain the time-of-flight (TOF) distributions, which we convert to energy spectra by applying the appropriate Jacobians. The detector is rotatable in the plane defined by the surface normal and the incident H/D atom beam allowing to measure TOF distributions at various final scattering angles ϑ_f . The used Ge crystal is undoped with a purity of 99.999%. The Ge(111) surface was cleaned with cycles of Ar⁺ ion sputtering and annealing at $\sim 670^\circ\text{C}$. The cleanliness and c(2×8) structure of the surface is validated by Auger electron spectroscopy and low-energy electron diffraction.

Theoretical methods

To perform theoretical simulations, a previously constructed NN-PES was improved and used for the D@Ge(111)c(2×8) system, and MD simulations were performed. For the MD simulations, the reconstructed Ge(111)c(2×8) surface was modeled using the c(2×8) surface unit cell, see Figure 1b. Details on the density functional theory (DFT) calculations, NN-PES, and MD simulations can be found in the Methods section of Ref. 18. Briefly, the Ge(111)c(2×8) slab consists of six mobile atomic layers plus two fixed layers with the bottom layer capped with H. The experimental lattice constant of 5.6575 Å²³ was used in the calculation. The supercell contains 148 atoms with a 3×1×1 k-grid. The Perdew–Burke–Ernzerhof functional²⁴ was used, and the core

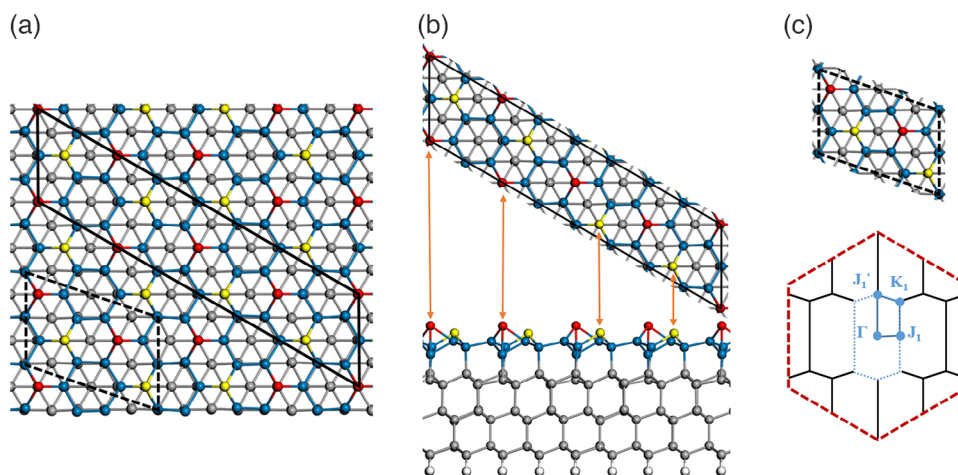


FIGURE 1 Top and side views of the Ge(111) $c(2\times 8)$ surface structure and surface Brillouin zone. Panel (a) shows the Ge(111) $c(2\times 8)$ surface structure in top view with marked $c(2\times 8)$ surface unit cell (black solid line) and $c(2\times 8)$ primitive surface unit cell (black dashed line). The red, yellow, blue, and gray balls represent adatoms, rest atoms, saturated atoms, and sublayer atoms, respectively. Panel (b) shows the $c(2\times 8)$ surface unit cell used in MD simulations in top and side view. The black line in the top view represents the periodic boundary. The white balls are H atoms used to terminate unsaturated Ge atoms of the lowermost layer in the theoretical model. Orange arrows point to adatoms and rest atoms in the front row of the side view representation. Panel (c) shows the $c(2\times 8)$ primitive surface unit cell as well as a schematic of the (1×1) (red dashed lines) and $c(2\times 8)$ primitive (blue dotted lines) surface Brillouin zones.

electrons were treated with the augmented project wave method.²⁵ About 6000 points were added to the original dataset to cover more configuration space and the newly fitted NN-PES has a root mean square error of about 80 meV/cell (or 0.8 meV/atom). For each experimental condition, 400,000 trajectories were calculated to achieve sufficient statistics and the error due to statistical sampling is negligible. These trajectories were initiated with conditions mimicking the experimental conditions and only scattered trajectories within $\pm 20^\circ$ of the incidence plane were collected to imitate the in-plane experimental detection. For the energy-loss spectra, a polar acceptance angle of $\pm 2.5^\circ$ was chosen. For one experimental condition, a few percent of the overall trajectories contribute to the energy-loss spectrum.

To gain insight into the change of local electronic structures of specific surface sites upon hydrogen impact, we computed the band structures of the clean Ge(111) $c(2\times 8)$ surface in a primitive cell (one-half the size of the Ge(111) $c(2\times 8)$ cell, see Figure 1c)²⁶ and the ones with an H atom adsorbed at adatom or rest atom site. Spin-polarized DFT calculations were performed using the Vienna Ab initio Simulation Package (VASP)^{27,28} with a Meta Simple (MS2)²⁹ exchange-correlation functional at the meta-generalized gradient approximation (meta-GGA) level. This MS2 functional was chosen differently from that used for generating the NN-PES, because it yields similar band structures with a finite band gap for the Ge(111) $c(2\times 8)$ surface (0.32 eV) as predicted by the more advanced yet much more costly hybrid functional (HSE06).³⁰ The plane-wave kinetic energy cutoff was 400 eV and the Brillouin zone was sampled by a $6 \times 2 \times 1$ Gamma-centered k -point grid. All adsorption geometries have been reoptimized with the MS2 functional and the same experimental lattice constant for band structure calculations. The suggested k -path in band structure calculations was along the Γ - J_1 - K_1 - J_1' - Γ symmetry directions in the Brillouin zone of the clean surface. The VASPKIT code³¹ was used for post-processing of the VASP calculated data. Other settings of

the slab model are identical to those used for generating the training data of the NN-PES, as detailed in Ref. 18. A more complete theoretical analysis of this system will be described in a forthcoming publication.

RESULTS

Figure 2 shows experimental translational energy-loss distributions for H and D atoms scattered from Ge(111) $c(2\times 8)$ with incidence energies, E_i , of approximately 1 eV (Figure 2a) and 2 eV (Figure 2b). At both incidence energies, bimodal energy-loss distributions are obtained for both isotopes. One channel shows low energy loss, while the other channel shows high energy loss with an onset close to the surface band gap of the Ge(111) $c(2\times 8)$ surface of 0.49 eV (marked by the vertical black dashed lines in Figure 2). We note that the value of the surface band gap was measured at a surface temperature of 30 K,³² whereas our measurements were performed at 300 K. Nevertheless, a similar, slightly lower, value of the surface band gap is expected at 300 K since the reconstruction of the surface remains the same. The H atom's low energy-loss channel was previously assigned to a mechanical interaction that can be described within an adiabatic model, whereas the high energy-loss channel is presumably formed by H atoms that induced electronic excitation of the surface.¹⁸

The two channels show different isotope effects. While the adiabatic channel shifts toward higher energy losses for deuterium, the high energy-loss channel shows no significant isotope effect. Also shown in Figure 2 are the ratios of the adiabatic to the nonadiabatic channel obtained at the specified experimental conditions. The branching ratio is nearly independent of isotopic substitution. For both isotopes, the nonadiabatic channel is strongly promoted by incidence translational energy.

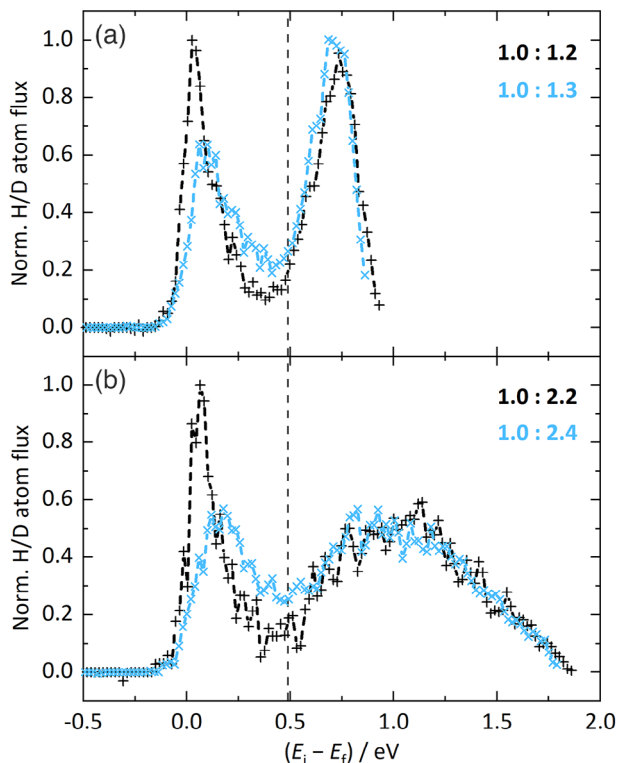


FIGURE 2 Experimental translational energy-loss distributions of H and D atoms scattered from Ge(111)c(2×8). The polar incidence and scattering angles ϑ_i and ϑ_f were both 45° and the incident atoms travel along the $[\bar{1}10]$ surface direction. The surface temperature T_S was 300 K. Experimental data for the two isotopes are shown for translational incidence energies of $E_{i,H} = 0.99$ eV and $E_{i,D} = 0.94$ eV (a) as well as $E_{i,H} = 1.92$ eV and $E_{i,D} = 1.87$ eV (b) for H (black) and D (blue), respectively. The band gap of the surface is 0.49 eV and indicated by the vertical dashed line. The experimentally obtained ratio of the low energy-loss channel to the high energy-loss channel, separated by the value of the surface band gap, appears in each panel for both isotopes, H (black) and D (blue). All curves are normalized to the integrated signal.

Figure 3 shows the comparison of the experimental data to the results of electronically adiabatic MD simulations for H and D atoms scattered at the specular angle. The MD simulations reproduce the adiabatic channel for both isotopes quite well. Additionally, vertical dotted lines show the energy losses predicted by a line-of-centers binary collision model for both isotopes and incidence energies. These values are close to the peaks of the experimentally and theoretically obtained distributions. The observed isotope effect for the adiabatic channel is well reproduced by the MD simulations. For both H and D atom scattering, the high energy-loss feature is not accounted for by the adiabatic MD simulation.

In Figure 4, we present polar plots that show energy-resolved angular distributions of the scattered atoms. Experimental data (Figure 4a,b) are compared to the results of adiabatic MD simulations (Figure 4c,d). Incidence translational energies of $E_{i,H} = 0.99$ eV and $E_{i,D} = 0.94$ eV for H and D, respectively, were used. In Figure 4a,b, black dotted lines show the expected minimal energy loss for the exci-

tation of an electron across the band gap of the surface, separating the adiabatic channel from the nonadiabatic channel for scattered H and D atoms. The adiabatic channel shows a broad angular distribution. The nonadiabatic channel exhibits a narrower angular distribution than the adiabatic feature for both isotopes. Again, the ratio of the nonadiabatic channel to the adiabatic channel is only slightly larger for D compared to H. The results of MD simulations (Figure 4c,d) reproduce the broad angular distributions of the adiabatic channels, while the nonadiabatic channel is absent. In Figure 5, the data given in Figure 4 are further analyzed and direct comparisons of the angle-integrated translational energy loss and energy-integrated angular distributions are shown for both isotopes. The energy loss of the adiabatic channel is well reproduced by the MD simulations. The angular distributions of the adiabatic channel obtained from experiment and theory show slight differences but still compare fairly well. In this representation, the different angular distributions of the adiabatic and nonadiabatic channels are especially pronounced: the angular distribution of the nonadiabatic channel is narrower.

DISCUSSION

A bimodal energy-loss distribution is observed for both H and D atoms scattered from the semiconducting Ge(111)c(2×8) surface. Both scattering channels show distinct isotope effects. We will first discuss the isotope effect on the energy loss and the angular distribution of the adiabatic channel, followed by the isotope effect on the nonadiabatic channel and finally, we will discuss the isotope effect on the branching ratio between both channels. We focus on the scattering dynamics of the nonadiabatic channel that has not yet been characterized theoretically.

Figure 2 reveals a small isotope effect on the energy loss of the adiabatic channel that is reproduced by both the adiabatic MD simulations and a simple binary collision model, as shown in Figure 3. The amount of transferred energy is larger for D than for H. This can be attributed to the higher mass of the D atoms compared to H leading to a more efficient energy transfer during the mechanical interaction with the Ge surface atoms. As shown in Figures 4 and 5, the angular distributions are broad and similar for both isotopes and fairly well reproduced by MD simulations. Overall, the isotope effect of the adiabatic channel reflects the expectations for a mechanical interaction and confirms the prior interpretation.

The observed energy loss of the nonadiabatic channel is very similar for both isotopes, see Figure 2. The value of the surface band gap of Ge(111)c(2×8) seems to determine the onset of the energy-loss distribution for both isotopes. Also, the shape and the peak of the energy-loss distributions are nearly identical for both isotopes. This is somewhat surprising, since one might expect—for example, within and electronic friction picture—different EHP excitation spectra for the two isotopes, with a smaller EHP excitation probability for D atoms.⁸ Furthermore, the angular distributions of the nonadiabatic channel, which are considerably narrower than those of the adiabatic channel at 1 eV, are very similar for both isotopes, as shown in Figures 4 and 5.

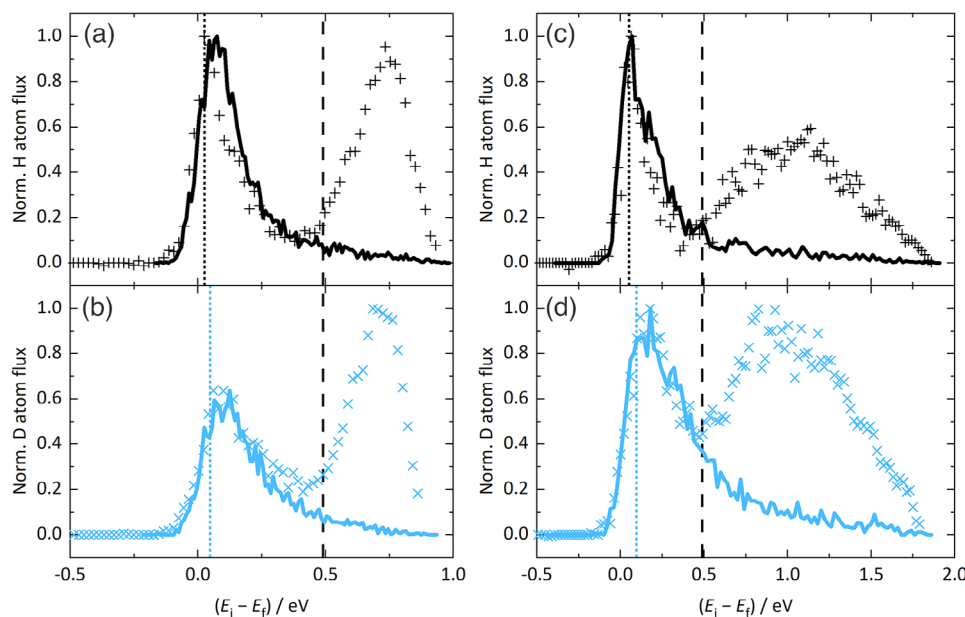


FIGURE 3 Comparison of experimental data to the results of adiabatic MD simulations for H and D atoms scattering from Ge(111)c(2×8) at the specular angle. Translational energy-loss distributions for H (black) and D (blue) atoms are shown for incidence translational energies of $E_{i,H} = 0.99$ eV (a) or $E_{i,H} = 1.92$ eV (c) and $E_{i,D} = 0.94$ eV (b) or $E_{i,D} = 1.87$ eV (d), respectively. The experimental conditions are the same as in Figure 2. Experimental data (+, ×) are compared to the results of adiabatic MD simulations (solid lines). All experimental curves are normalized to the peak intensity. The MD curves are scaled to fit the adiabatic channel. The band gap of the surface is 0.49 eV and indicated by the vertical black dashed lines. Dotted lines represent the energy loss predicted by a line-of-centers binary collision model: $E_i - E_f = E_i \cos^2[(\vartheta_i + \vartheta_f)/2] \times [1 - (m_H - m_{Ge})^2 / (m_H + m_{Ge})^2]$.

Our observations suggest that the shape of the energy-loss distribution of the nonadiabatic channel is controlled by the density of states of the involved surface states. The narrow angular distribution could be caused by the fact that a specific surface site has to be hit in a certain geometry for an EHP excitation to occur.

The ratios of the nonadiabatic channel to the adiabatic channel are given in Figure 4a,b for both isotopes for incidence translational energies of about 1 eV. A similar branching ratio is observed for H and D, with a slightly stronger nonadiabatic channel for the heavier isotope. We want to highlight that the probability to initiate electronic excitation during a collision with the surface is nearly equal for H and D at a given incidence energy. From past work, one expects a smaller EHP excitation probability for deuterium. In chemicurrent experiments with Schottky diodes, for example, differences in EHP detection efficiency are observed for impinging H and D atoms.^{13–15} Such an isotope effect is clearly not seen in the current study, leading to the conclusion that the observed branching ratio cannot be determined by the probability to induce nonadiabatic processes. It has to be related to another property of the system. To understand this, we next consider the surface electronic structure.

The formally defined Ge(111) surface structure is highly unstable, as each atom of the first surface layer exhibits a dangling bond. This situation is remedied by the formation of a c(2×8) reconstructed surface shown in Figure 1. The surface consists of 0.25 monolayer adatoms (shown in red) each possessing a single dangling bond and bound to three saturated atoms of the first layer (shown in blue). Additional

dangling bonds are located at rest atoms in the first layer (shown in yellow). The surface is further stabilized by the transfer of one dangling bond electron from adatoms to rest atoms, which are present in equal quantities.³³ Also note that there are also second layer (shown in blue) and sublayer (shown in gray) tetravalent Ge atoms.

Figure 6 shows calculations of the electronic structure of the surface and how it is changed in the presence of an H atom. The left panel shows the calculated band structure of the pristine Ge(111)c(2×8) surface, whereas the other two panels show the band structures obtained for H adsorbed on a Ge adatom (middle panel) and on a Ge rest atom (right panel). Note that in Figure 6, red and blue colors are used to denote nondegenerate spin states, whereas green curves are used to denote degenerate spin states. We find that for the pristine surface, the highest occupied (valence band) surface state is doubly occupied and localized at rest atoms, whereas the lowest unoccupied (conduction band) surface state is localized at adatoms. It is, therefore, reasonable to assume that the promotion of an electron from the valence band to the conduction band via an H atom collision at the surface involves the transfer of an electron from a rest atom to an adatom. Figure 6 shows that H binding to a Ge rest atom results in a population of the previously unoccupied adatom surface state (bold red line in Figure 6), suggesting strongly that an H atom collision at a rest atom site can lead to electron transfer to an adatom site, promoting an electron from the valence to the conduction band. Hence, we hypothesize that when an H atom forms a 2-electron bond to a rest atom, the charge is simultaneously transferred back to an adatom, bringing the

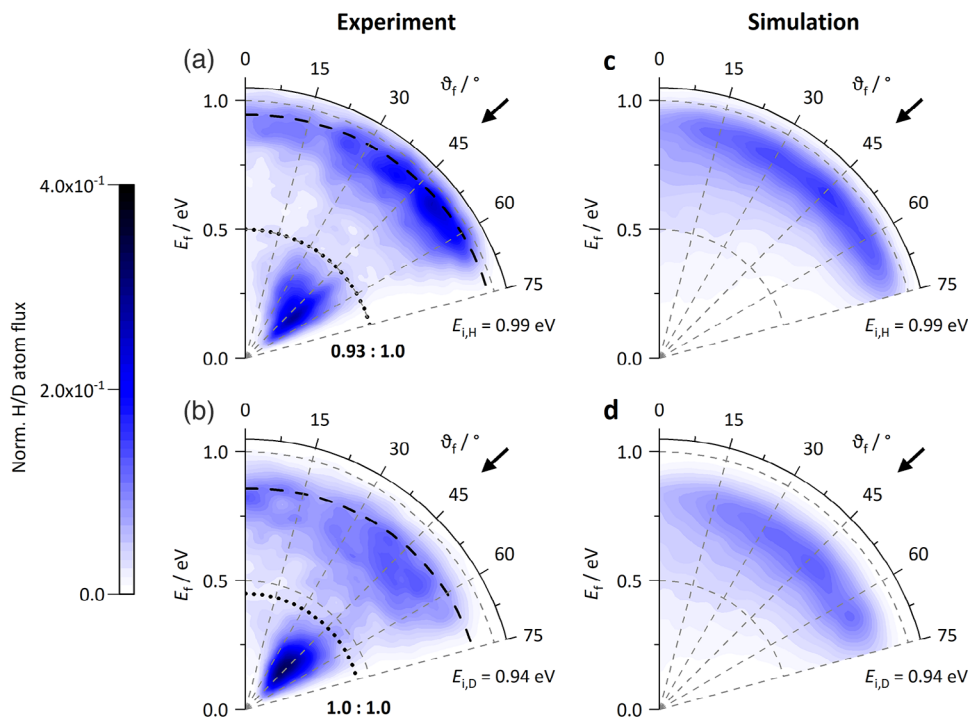


FIGURE 4 Energy-resolved angular distributions observed for H and D atom scattering from Ge(111)c(2×8). Distributions derived from in-plane scattering flux are shown for H (a & c) and D (b & d) atoms with incidence translational energies $E_{i,H} = 0.99 \text{ eV}$ (a & c) and $E_{i,D} = 0.94 \text{ eV}$ (b & d) at an incidence angle $\vartheta_i = 45^\circ$. Specular scattering angles are marked by black arrows. The surface temperature was $T_S = 300 \text{ K}$. Experimental results (a & b) are compared to MD simulations (c & d). The MD simulations reproduce the behavior of the adiabatic channel only. To construct the experimental plots, data were recorded in 5° increments from $\vartheta_f = 0^\circ$ to 75° . Bold numbers show the ratios of the experimentally observed nonadiabatic channel (left) to the adiabatic channel (right). Each experimental distribution is normalized and the MD simulations are scaled to the respective experiment such that the integrated adiabatic channels are equal in both. The black dashed lines represent the final energy predicted by a line-of-centers binary collision model: $E_f = E_i [1 - \cos^2[(\vartheta_i + \vartheta_f)/2] \times [1 - (m_H - m_{Ge})^2 / (m_H + m_{Ge})^2]]$. The black dotted lines indicate the final energy of H and D atoms, respectively, that lost 0.49 eV during the interaction with the surface, corresponding to the value of the surface band gap.

previously unoccupied surface state below the Fermi level. Once the H atom again leaves the surfaces (a process requiring only $\sim 25 \text{ fs}$), electron population remains in this adatom surface state, which once again belongs to the conduction band. This viewpoint can explain the lack of an isotope effect as electronic excitation probabilities are determined by the likelihood to hit a specific surface atom, which is equal for both isotopes.

The changes in electronic structure induced by an H atom collision can be more clearly seen in Figure 7. When H binds to the Ge adatom (Figure 7a), the previously unoccupied dangling bond now forms the H-Ge bond with the electron of hydrogen atom, borrowing electron density from nearby saturated Ge atoms. This leads to a drop of the Fermi energy. In contrast, Figure 7b shows the difference in charge density between the pristine surface and the surface with an H atom bonding to a rest atom. The calculations reveal that the additional electron is transferred to an adatom site.

H atom-induced electron transfer from rest to adatoms is also consistent with the results of scanning tunneling microscopy experiments, in which a charge transfer from the rest to the adatom upon H adsorption on the rest atom site was observed.^{34,35} As a consequence, the transferred electron fills the unoccupied adatom dangling bond band

originally in the conduction band, making it fall into the valence band. Interestingly, since there is only one additional electron, the drop of the energy level occurs only in one spin manifold. Note that in the case of an H atom binding at the adatom, no such charge transfer between ad and rest atoms is seen (see Figure 7a). Of course, electronically nonadiabatic dynamics calculations are needed. Nevertheless, the process just described could involve a crossing of electronic states during the collision of a hydrogen atom.

Site-specific scattering is also expected to produce a narrower angular distribution of the scattered H atoms. This might well explain why the electronically nonadiabatic channel exhibits a much narrower angular distribution than does the adiabatic one, which is not site-specific. Scattering from each of the surface sites contributes to the shape of the overall angular distribution. The potential, geometry, energy transfer, and sticking probability may differ for different surface sites, all of which will affect the contribution of one site to the overall angular distribution. While adiabatic MD simulations are not capable of reproducing the observed angular distributions, we can nevertheless analyze whether the angular distributions depend strongly on the scattering site. Such an analysis shows that the angular distribution of H atoms scattered from the adatom site shows the best agreement

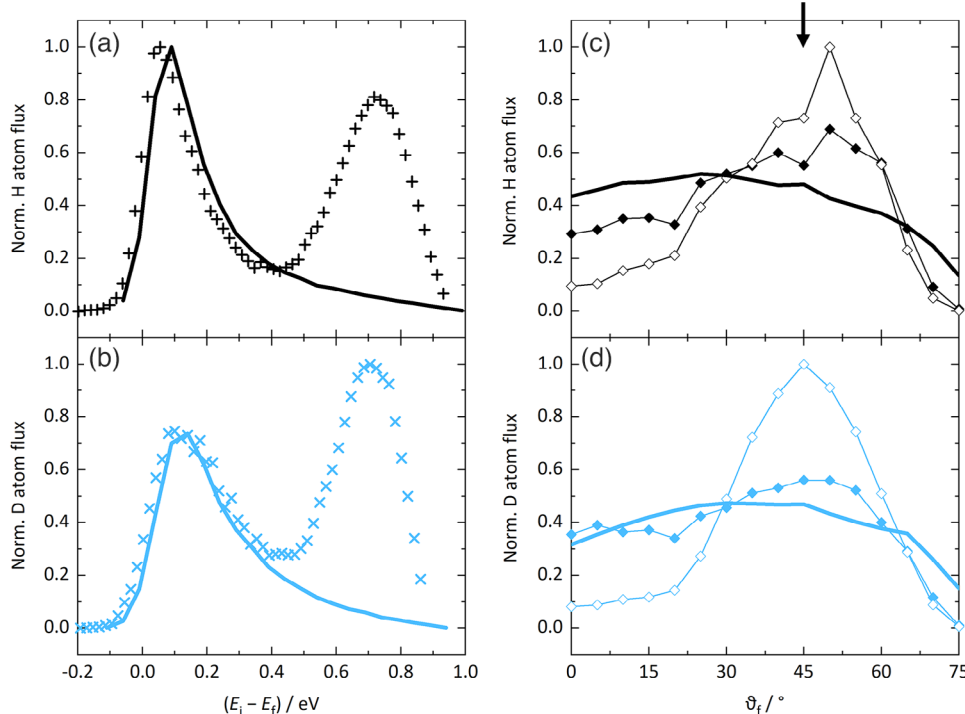


FIGURE 5 Comparison of energy loss and angular distributions for H and D atoms scattering from Ge(111)c(2×8). Angle-integrated translational energy-loss distributions (a & b) and energy-integrated angular distributions (c & d) derived from data given in Figure 4 are shown for H (a & c) and D (b & d) atoms with incidence translational energies $E_{i,H} = 0.99$ eV (a & c) and $E_{i,D} = 0.94$ eV (b & d) at an incidence angle $\vartheta_i = 45^\circ$. All other experimental conditions are the same as in Figure 4. To construct the angle-integrated energy-loss distributions, angle-resolved energy-loss distributions recorded in 5° increments from $\vartheta_f = 0^\circ$ to 75° , given in Figure 4, were summed up. The curves are further normalized to the peak intensity of the experimental data. To construct the energy-integrated angular distributions, the energy-loss distribution at each scattering angle was summed up in energy space; however, in the case of the experimental data, divided into the adiabatic channel (filled diamonds) and the nonadiabatic channel (open diamonds), separated by the surface band gap. The curves are normalized to the peak intensity of the nonadiabatic channel. The results from MD simulations are shown by solid lines. The specular scattering angle is marked by an arrow at the top of panel c.

with the observed angular distribution of the adiabatic channel. However, scattering from all surface sites exhibited rather broad angular distributions, and only small site-dependent differences are seen.

For both isotopes, the nonadiabatic channel is strongly promoted by incidence translational energy, as shown in Figure 2. Three factors have to be considered within the context of this observation. First, higher energy means higher speed which is known to promote nonadiabatic effects. However, since we see nearly no isotope effect on the branching ratio, we also do not expect a large effect due to an increased speed of the atoms. Second, higher translational energies make additional interband transitions energetically possible.³³ Additional transitions, which might not be constrained to certain surface sites, become accessible. The broadening of the angular distributions when going from 1 to 2 eV incidence energy (see Ref. 18 for H) is consistent with this interpretation. Third, the incidence energy dependence of the sticking probability can be expected to be different for both scattering channels and thus for different surface sites. As shown in Ref. 18, more integrated signal is observed for higher incidence energies, meaning that the sticking probability decreases with increasing incidence energy. Additionally, it was observed that the difference in signal is mainly due

to the nonadiabatic channel. Overall, the change of the branching ratio with increasing incidence translational energy—promoting the nonadiabatic channel—appears to be due to additional interband excitations that become accessible combined with a reduced sticking probability mainly attributed to the nonadiabatic channel.

As mentioned above, a quantitative theoretical model, capable of describing the experimental observations, is still lacking. An earlier attempt to use an electronic friction model failed to capture the bimodal energy-loss distributions,¹⁸ underscoring the inadequacy of the perturbative treatment of nonadiabatic transitions. Nevertheless, the evidence presented in this paper strongly suggests a site-specific process is responsible for the nonadiabatic excitation of electrons from the valence band to the conduction band. Specifically, we envision that as the H/D atom approaches the Ge surface, its high speed causes a strong perturbation of the local electronic structure at the impact site, which leads to a mixing of occupied and unoccupied surface states. The mixing enables the population of states lying above the surface band gap, converting the kinetic energy of the incident atom to electronic excitation. Finally, the atom is scattered from the surface with significant energy loss.

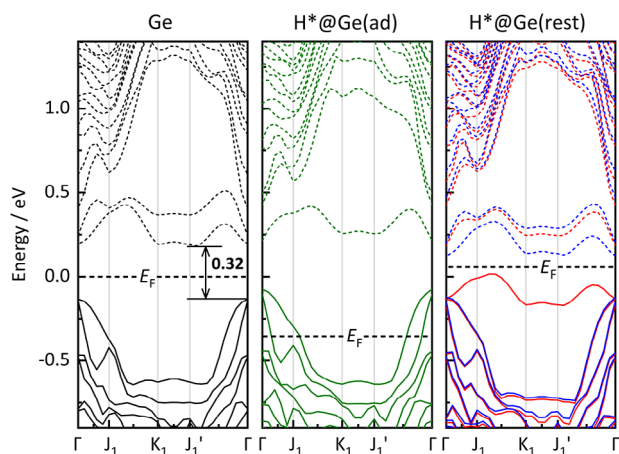


FIGURE 6 Change of band structures of Ge(111)c(2×8) upon H adsorption on different surface sites. Comparison of band structures of the Ge(111)c(2×8) surface (Ge, left), H adsorbing on the Ge adatom (H*@Ge(ad), middle), and on the Ge rest atom (H*@Ge(rest), right). Horizontal black dashed lines represent the Fermi level in different cases on the same energy scale. The calculated band gap of Ge(111)c(2×8) between conduction (dashed line) and valence band (solid line) is marked in the left panel by a vertical arrow (in eV). Spin-up and spin-down band structures are identical for the Ge and H*@Ge(ad) cases, but not for the H*@Ge(rest) case and thus shown in blue and red, respectively. Note that H adsorption on the adatom only results in a downward shift of the Fermi level, while on the rest atom, H atom adsorption causes a flip of one energy level from the conduction band to valence band (bold red).

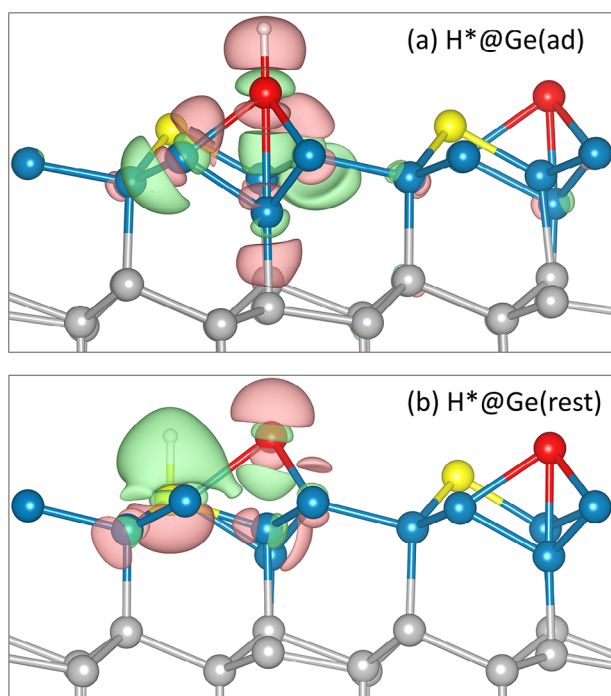


FIGURE 7 Differential charge density. Charge density of H*@Ge(ad) (a) and H*@Ge(rest) (b) minus that of the pristine Ge surface. Net charge gain is shown in pink and loss in green. The iso-surface value is 0.005 eV/\AA^3 . Red, yellow, blue, and gray balls represent adatoms, rest atoms, saturated atoms, and sublayer atoms, respectively, the same as in Figure 1.

CONCLUSIONS

In summary, we used experimental data and results of electronically adiabatic MD simulations to investigate inelastic D atom scattering from Ge(111)c(2×8) and to study the isotope effect by comparing D to H atom scattering. The results confirm the existence of two channels that show fundamentally different scattering mechanisms: D and H atoms can either experience a mechanical interaction with the surface well described within the Born–Oppenheimer approximation (BOA) or a nonadiabatic interaction leading to electronic excitation across the surface band gap. To fully describe the experimentally observed energy loss and to understand the dynamics in detail, MD simulations beyond the limits of the BOA will be needed in the future. However, based on the observed branching between both scattering channels, which is only marginally influenced by isotopic substitution, we propose a surface site-specific energy transfer mechanism, which is supported by the change of the electronic band structure upon H adsorption at different surface sites. The experimental observations presented here pose a challenge to theory in providing a quantitative characterization of the nonadiabatic dynamics involving the excitation of EHPs across the semiconductor band gap.

AUTHOR CONTRIBUTIONS

A.M.W. and O.B. conceived the project. O.B. supervised the experiment and B.J. and H.G. supervised the theoretical simulations. K.K. performed the experiments. L.Z. and Y.W. performed the simulations. K.K. and Y.W. analyzed the data. K.K. and O.B. wrote the manuscript with feedback from A.M.W., L.Z., Y.W., B.J., and H.G.

ACKNOWLEDGMENTS

We thank Alexander Kandratsenka for the helpful discussions. O.B. and A.M.W. acknowledge support from the Deutsche Forschungsgemeinschaft (DFG) under SFB 1073, project A04 (217133147), and from the DFG, the Ministerium für Wissenschaft und Kultur, Niedersachsen, and the Volkswagenstiftung under grant number INST 186/902-1. H.G. acknowledges support from the National Science Foundation under grant nos. CHE-1951328 and CHE-2306975. B.J. acknowledges support from the K. C. Wong Education Foundation under grant number GJTD-2020-15. A.M.W. and H.G. acknowledge support from the Alexander von Humboldt Foundation. A.M.W. thanks the Max Planck Society for the Advancement of Science. B.J. thanks Dr. Wei Hu for the helpful discussion on band structure calculations.

Open access funding enabled and organized by Projekt DEAL.

CONFLICT OF INTEREST STATEMENT

The authors declare no conflict of interest.

DATA AVAILABILITY STATEMENT

The data that support the findings of this study are available from the corresponding author upon reasonable request.

ORCID

Kerstin Krüger  <https://orcid.org/0000-0002-5826-2674>

Bin Jiang  <https://orcid.org/0000-0003-2696-5436>

Hua Guo  <https://orcid.org/0000-0001-9901-053X>

Alec M. Wodtke  <https://orcid.org/0000-0002-6509-2183>

Oliver Bünermann  <https://orcid.org/0000-0001-9837-6548>

PEER REVIEW

The peer review history for this article is available at <https://www.webofscience.com/api/gateway/wos/peer-review/10.1002/ntls.20230019>

ETHICS STATEMENT

The authors confirm that they have followed the ethical policies of the journal.

REFERENCES

- Rettner CT. Dynamics of the direct reaction of hydrogen-atoms adsorbed on Cu(111) with hydrogen-atoms incident from the gas-phase. *Phys Rev Lett.* 1992;69(2):383-386.
- Rettner CT, Auerbach DJ. Quantum-state distributions for the HD product of the direct reaction of H(D)/Cu(111) with D(H) incident from the gas phase. *J Chem Phys.* 1996;104(7):2732-2739.
- McMaster MC, Madix RJ. Kinetic isotope effect in direct ethane dissociation on Pt(111). *Surf Sci.* 1993;294(3):420-428.
- Nesbitt A, Harder R, Golichowski A, Herrmann G, Snowdon KJ. Isotope effects in the dissociative dynamics of energetic hydrogen scattered from Cu(111) under glancing angles of incidence. *Chem Phys.* 1994;179(2):215-226.
- Nienhaus H, Bergh HS, Gergen B, Majumdar A, Weinberg WH, McFarland EW. Electron-hole pair creation at Ag and Cu surfaces by adsorption of atomic hydrogen and deuterium. *Phys Rev Lett.* 1999;82(2):446-449.
- Romm L, Citri O, Kosloff R, Asscher M. A remarkable heavy atom isotope effect in the dissociative chemisorption of nitrogen on Ru(001). *J Chem Phys.* 2000;112(19):8221-8224.
- Bondarchuk O, Kim YK, White JM, Kim J, Kay BD, Dohnalek Z. Surface chemistry of 2-propanol on TiO₂(110): low- and high-temperature dehydration, isotope effects, and influence of local surface structure. *J Phys Chem C.* 2007;111(29):11059-11067.
- Kandratsenka A, Jiang HY, Dorenkamp Y, et al. Unified description of H-atom-induced chemisorption and inelastic scattering. *Proc Natl Acad Sci U S A.* 2018;115(4):680-684.
- Kaufmann S, Shuai Q, Auerbach DJ, Schwarzer D, Wodtke AM. Associative desorption of hydrogen isotopologues from copper surfaces: characterization of two reaction mechanisms. *J Chem Phys.* 2018;148(19):194703.
- Dorenkamp Y, Volkmann C, Roddatis V, Schneider S, Wodtke AM, Bünermann O. Inelastic H atom scattering from ultrathin aluminum oxide films grown by atomic layer deposition on Pt(111). *J Phys Chem C.* 2018;122(18):10096-10102.
- Head-Gordon M, Tully JC. Molecular dynamics with electronic frictions. *J Chem Phys.* 1995;103(23):10137-10145.
- Nienhaus H. Electronic excitations by chemical reactions on metal surfaces. *Surf Sci Rep.* 2002;45(1-2):3-78.
- Krix D, Nunthel R, Nienhaus H. Generation of hot charge carriers by adsorption of hydrogen and deuterium atoms on a silver surface. *Phys Rev B.* 2007;75(7):073410.
- Mildner B, Hasselbrink E, Dising D. Electronic excitations induced by surface reactions of H and D on gold. *Chem Phys Lett.* 2006;432(1-3):133-138.
- Schindler B, Dising D, Hasselbrink E. Electronic excitations induced by hydrogen surface chemical reactions on gold. *J Chem Phys.* 2011;134(3):034705.
- Dorenkamp Y, Jiang HY, Kockert H, et al. Hydrogen collisions with transition metal surfaces: universal electronically nonadiabatic adsorption. *J Chem Phys.* 2018;148(3):034706.
- Jiang HY, Dorenkamp Y, Krüger K, Bünermann O. Inelastic H and D atom scattering from Au(111) as benchmark for theory. *J Chem Phys.* 2019;150(18):184105.
- Krüger K, Wang Y, Tödter S, et al. Hydrogen atom collisions with a semiconductor efficiently promote electrons to the conduction band. *Nat Chem.* 2023;15(3):326-331.
- Alducin M, Diez Muiño R, Juaristi JI. Non-adiabatic effects in elementary reaction processes at metal surfaces. *Prog Surf Sci.* 2017;92(4):317-340.
- Bünermann O, Kandratsenka A, Wodtke AM. Inelastic scattering of H atoms from surfaces. *J Phys Chem A.* 2021;125(15):3059-3076.
- Bünermann O, Jiang HY, Dorenkamp Y, Auerbach DJ, Wodtke AM. An ultrahigh vacuum apparatus for H atom scattering from surfaces. *Rev Sci Instrum.* 2018;89(9):094101.
- Schnieder L, Seekampahn K, Liedeker F, Steuwe H, Welge KH. Hydrogen-exchange reaction H + D₂ in crossed beams. *Faraday Discuss.* 1991;91:259-269.
- Weast RC. *CRC Handbook of Chemistry and Physics.* CRC Press; 1987.
- Perdew JP, Burke K, Ernzerhof M. Generalized gradient approximation made simple. *Phys Rev Lett.* 1996;77(18):3865-3868.
- Blöchl PE. Projector augmented-wave method. *Phys Rev B.* 1994;50(24):17953-17979.
- Smith PV, Radny MW, Shah GA. Density functional study of the Ge(111)c(2×8) surface using the modified Becke-Johnson exchange potential with LDA correlation and spin-orbit interactions. *RSC Adv.* 2014;4(89):48245-48253.
- Kresse G, Furthmüller J. Efficient iterative schemes for ab initio total-energy calculations using a plane-wave basis set. *Phys Rev B.* 1996;54(16):11169-11186.
- Kresse G, Furthmüller J. Efficiency of ab-initio total energy calculations for metals and semiconductors using a plane-wave basis set. *Comput Mater Sci.* 1996;6(1):15-50.
- Sun J, Haunschild R, Xiao B, Bulik IW, Scuseria GE, Perdew JP. Semilocal and hybrid meta-generalized gradient approximations based on the understanding of the kinetic-energy-density dependence. *J Chem Phys.* 2013;138(4):044113.
- Krukau AV, Vydrov OA, Izmaylov AF, Scuseria GE. Influence of the exchange screening parameter on the performance of screened hybrid functionals. *J Chem Phys.* 2006;125(22):224106.
- Wang V, Xu N, Liu J-C, Tang G, Geng W-T. VASPKIT: a user-friendly interface facilitating high-throughput computing and analysis using VASP code. *Comput Phys Commun.* 2021;267:108033.
- Feenstra RM, Lee JY, Kang MH, Meyer G, Rieder KH. Band gap of the Ge(111)c(2×8) surface by scanning tunneling spectroscopy. *Phys Rev B.* 2006;73(3):035310.
- Razado-Colambo I, He JP, Zhang HM, Hansson GV, Uhrberg RIG. Electronic structure of Ge(111)c(2×8): STM, angle-resolved photoemission, and theory. *Phys Rev B.* 2009;79(20):205410.
- Klitsner T, Nelson JS. Site-specific hydrogen reactivity and reverse charge-transfer on Ge(111)-c(2×8). *Phys Rev Lett.* 1991;67(27):3800-3803.
- Razado IC, Zhang HM, Hansson GV, Uhrberg RIG. Hydrogen-induced metallization on Ge(111) c(2×8). *Appl Surf Sci.* 2006;252(15):5300-5303.

How to cite this article: Krüger K, Wang Y, Zhu L, et al. Isotope effect suggests site-specific nonadiabaticity on Ge(111)c(2×8). *Nat Sci.* 2024;4:e20230019. <https://doi.org/10.1002/ntls.20230019>